

Abstract

The gender identification can be made to approximately 95% accuracy when all the bones that the skull consists of are present and well preserved. A difficult problem that occurs for the medical examiner is that the favourable anatomical conditions are not often available. The large oval aperture, foramen magnum, which pierces the occipital bone that is situated at the back and lower cranium was measured, as evaluation of this region may be useful when examining a fragmented skull. The manual measurements are difficult to achieve and not often repeatable.

The preliminary investigation establishes an easily reproducible vision system based on the intelligent scissors system that will extrapolate the particular desired measurements from a 2D image of the foramen magnum. The initial study used 5 skulls from the UCD anthropological department to evaluate the robustness and accuracy of the system. Comparing them with the standard manual measurements were used to assess the accuracy of the system. Then using the depth from defocus method to obtain 3D images the 2D techniques for obtaining the data were transferred to evaluate the depth images.

Table of Contents

Abstract	1
Table of Figures.....	3
Chapter 1 : Introduction.....	4
1.1 Presentation of traditional methods.....	5
1.2 Problem and Motivation.....	8
Chapter 2: Livewire Background and Implementation.....	9
2.1 Livewire.....	9
2.1.1 Dynamic Programming, Graph search.....	10
2.2 Overview of the Final System.....	12
Chapter 3: Statistical Analysis of 3D data.....	13
3.1 Depth from Defocus.....	13
3.2 Statistical Analysis of 3D data - Orthographic View.....	15
3.2.1 Least Square Planar Fitting.....	15
3.2.2 Planar Projection.....	16
3.3 Image Pixel Dimensions.....	18
Chapter 4: Measurement Code.....	20
4.1 Initial Code.....	20
4.2 2D Information Acquisition.....	21
4.3 3D Range Acquisition.....	24
Chapter 5: Calibration.....	26
5.1 Scaling Factor.....	26
5.2 Testing the Scale.....	29
5.2.1 Testing the Scale for the Skull Images.....	30
5.3 Final Scale.....	31
Chapter 6: Testing.....	32
6.1 Determining Robustness.....	32
6.1.1 Slope Constraints.....	34
6.1.2 Robustness with respect to the Midsagittal Plane.....	35
6.2 2D Image Testing.....	39
6.3 3D Image Testing.....	41
6.3.1 Varying the angle of Projection.....	44
6.4 Gender Identification.....	44
6.4.1 Analysis of 2D Results for Identification.....	45
6.4.2 Analysis of 3D Results for Identification.....	48
Conclusion.....	51
References.....	52

Table of Figures

Figure 1: The Base of the Skull.....	5
Figure 2: Placement of midsagittal plane with respect to Foramen Magnum.....	6
Figure 3: Anomalies of Occipital Bone at Foramen Magnum.....	7
Figure 4: Flow Chart of <i>Livewire</i> 2D Dynamic Programme Graph Search Algorithm...	11
Figure 5: Flow Chart of the Vision System.....	12
Figure 6: Actively Illuminated Image and Computed Depth Image of Skull 6.....	14
Figure 7: Flow Chart of 3D Information Computation.....	14
Figure 8: Rotations constrained by the normal vector N to the object surface.....	16
Figure 9: 3D view demonstrating Orthographic projection.....	18
Figure 10: Image of Resizing Image Dialogue Box.....	19
Figure 11: Initial Result Images.....	23
Figure 12: Graphical Interface of the Additional Measurement Functions.....	25
Figure 13: Calibration Image 1 (Calib1.bmp).....	27
Figure 14: Calibration Image 2 (Calib2.bmp).....	28
Figure 15: 2D Results, LFM and WFM vs FMC.....	47
Figure 16: 2D Results, Estimated FMA and Actual Area vs FMC^2	47
Figure 17: 3D Results, LFM and WFM vs FMC.....	48
Figure 18: 3D Results, Estimated FMA and Actual Area vs FMC^2	49
Figure 19: Projected 3D Results, LFM and WFM vs FMC.....	49
Figure 20: Projected 3D Results, Estimated FMA and Actual Area vs FMC^2	50
Table 1: Calibration Results.....	30
Table 2: Length and Width Results and Coordinate Results for Skull 9.....	32
Table 3: Length and Width Results and Coordinate Results for Skull 9 tilted by 30^0	33
Table 4: Averaged Length and Width Results for Skulls 6, 11, 13 and 14.....	34
Table 5: Detecting LFM and WFM with 1 pixel difference between axis coordinates...	36
Table 6: Detecting LFM and WFM with 2 pixel difference between axis coordinates...	37
Table 7: Detecting LFM and WFM with 3 pixel difference between axis coordinates...	37
Table 8: Detecting LFM and WFM with 4 pixel difference between axis coordinates...	37
Table 9: Detecting LFM and WFM with 5 pixel difference between axis coordinates...	38
Table 10: Skull 6 2D Result.....	39
Table 11: Skull 9 2D Results.....	40
Table 12: Skull 11 2D Results.....	40
Table 13: Skull 13 2D Results.....	40
Table 14: Skull 14 2D Results.....	40
Table 15: Skull 6 3D Results.....	41
Table 16: Skull 9 3D Results.....	42
Table 17: Skull 11 3D Results.....	43
Table 18: Skull 13 3D Results.....	43
Table 19: Skull 14 3D Results.....	43
Table 20: Results from Best Angle for Projection for each Tilted Image.....	44
Table 21: Anthropologists Gender Identification of the Skulls.....	45
Table 22: Final 2D Results, Noting 11 and 13 has rotational errors.....	46
Table 23: Final 3D Results with No Orthographic View applied and Depth Estimation Errors.....	48

Chapter 1: Introduction

This project is in collaboration with the UCD forensic Anthropology and Research group. Forensic anthropology is the application of the science of physical anthropology to the legal process.

The identification of skeletal badly decomposed or otherwise, unidentified human remains are important for both legal and humanitarian reasons. Forensic anthropologists apply standard scientific techniques developed in physical anthropology to identify human remains, and to assist in the detection of crime. Forensic anthropologists frequently work in conjunction with forensic pathologists and homicide investigators to identify a dead body and discover evidence of foul play. In addition to assisting in locating and recovering suspicious remains, forensic anthropologists work to suggest the age, sex, ancestry, stature, and unique features of a deceased person from the skeleton.[1]

In forensic science and anthropology, the skull is more frequently and thoroughly investigated than any other section of the human skeleton. For this project the adult skull will be used to determine the gender. The human skull is a complex structure and it consists of the largest number of measurements and calculable indices than most other bones in the human skeleton. In particular the occipital region of the skull is of high interest.

Artificial Cranial Deformation is an unnatural forced human alteration of the skull. It permanently changes the original genetically defined cranial shape, altering frontal facial morphology and other cranial bones. [2] The occipital is a bone at the inferior and posterior aspect of the skull, due to its position it is often found undamaged in human remains. For the project measurements were taken at the cranial base of the skull as it has a number of features with proportions that may be gender specific.

The human skull can be used to determine race by evaluation and comparison of the anatomical and morphological skull feature variations. Thus there are significant

differences between Caucasoid, Mongoloid and Negroid skeletons through variations of statistical analysis. Success rates gender identification for Caucasoid skulls generally yield better results than Mongoloid or Negroid. It is important to note that in this project the Caucasoid skull is the only source of testing.

1.1 Presentation of traditional methods

The main objective of this project is to create an image processing based vision system that will take specific measurements, normally taken manually, from a digital image of the occipital area. In this section the traditional method for extrapolating the specific measurements will be addressed.

Occipital bone is situated at the back and lower cranium, it is trapezoidal in shape and curved on itself. It is also pierced by a large oval aperture i.e. the foramen magnum, through which the cranial cavity communicates with the vertebrae canal i.e. the spinal chord, as can be seen in the figure of the posterior of the skull. It is this area that will be measured for further statistical analysis. The figure 1 shows the skull viewed from an exterior viewpoint.

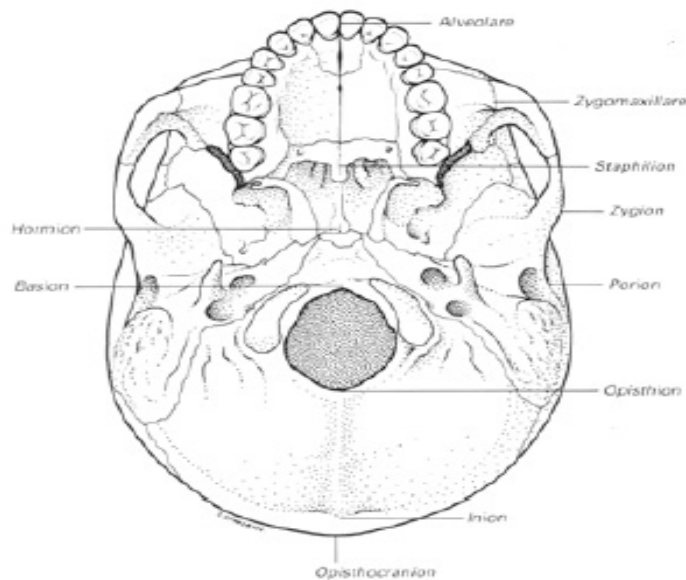


Figure 1: The Base of the Skull [3]

The task of this project was to take specific measurements from digital images. The program devised for this task will be tested for different Caucasoid skulls supplied by the University College Dublin, UCD, anthropological department. The measurements are morphological characteristics of the human skull that can help in gender identification. These measurements include the maximum length of the foramen magnum, LFM, and width of the foramen magnum, WFM. These distances are to be taken in a similar fashion to that of measuring with callipers.

To clarify the length and width are measured with respect to the midsagittal plane. It is an inter-hemispheric fissure bisecting the human body. This plane gives an approximate bilateral symmetry to the skull, as the skull is never perfectly symmetric. [4] The maximum internal length is measured along the plane. Where as the width is measured perpendicular to the plane. The clarification of this is shown in Figure 2.

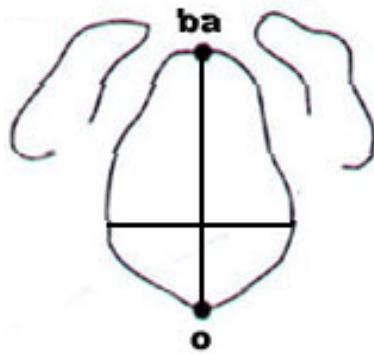


Figure 2: Placement of midsagittal plane with respect to Foramen Magnum Basion (ba) the midline point on the anterior margin and Opisthion(o) the midline point at the posterior margin of the foramen magnum.

A more difficult challenge is the measuring of the circumference of the foramen magnum, FMC. No two skulls are identically formed due to the mutational processes involved during DNA replication, and meiosis, i.e. sexual reproduction stage. [5] As can be seen in figure 2, particularly B and C, the circumference of the foramen magnum opening can be obstructed by occipital condyles depending on the skull shape.

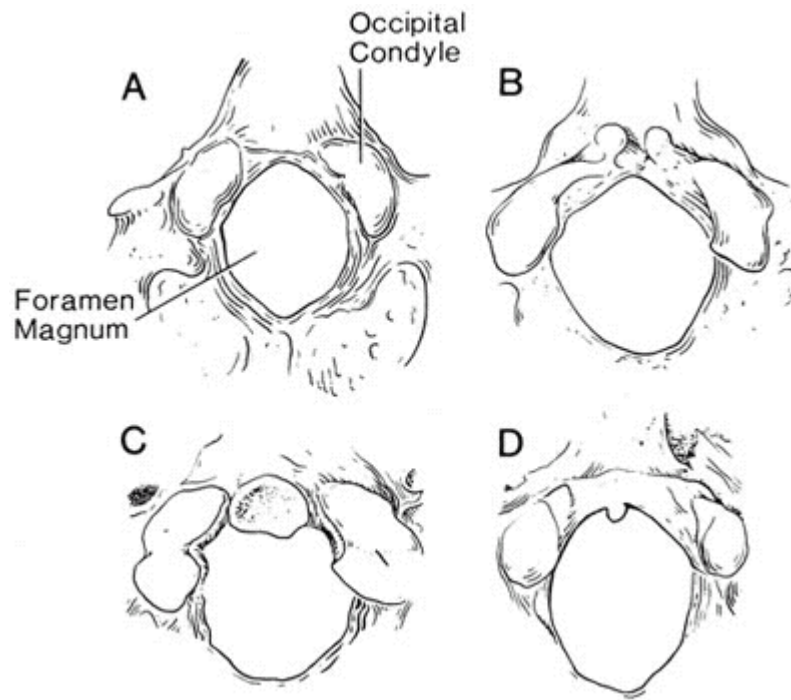


Figure 3: Anomalies of Occipital Bone at Foramen Magnum [6]

A. The usual appearance of occipital bone at the foramen magnum, B. Precondylar tubercles, C. Third occipital condyle and D. Ossification of the ligament of the odontoid process of the axis

The method that is manually applied to take the circumference measurement involves the use of a strip of paper, which is pressed around the edge of the foramen magnum circumference. The indentations that trace the shape are then used to record the distance that they cover over the paper. This rudimentary technique is in current use to determine the undulating edge surface of the foramen magnum.

Obtaining the fourth and final measurement of the area, FMA is easily done, once the circumference has been extrapolated. The area was obtained by using the following basic equation for the circumference of the circle,

$$circumference(circle) = 2 * \pi * R$$

As can be seen from the figure on the previous page the shape of the aperture may not actually be circular but is taken to be an approximation. This is then could be translated into the area formula,

$$area(circle) = \pi * R^2$$

There is another variation to this approach for finding area, which is documented in the Teixeira paper.[7] In this case the area is estimated by obtaining the medium value between the half measures of the length and width.

1.2 Problem and Motivation

The aim of this project was to produce an algorithm that is easily incorporated in an anthropologist's fieldwork. The hardware available may be limited. For example there may not be sufficient means of light control when taking an image and also a simple digital camera may be the only means of image acquisition. Also the reliability of such measurements for gender identification are quite low with normally about 80% accuracy. Ideally the introduction of a vision system may increase the robustness and relative accuracy of sex determination from the foramen magnum.

The methods used to acquire the measurements are quite elementary and with the circumference in particularly quite cumbersome. *Livewire* supplied the functionality required for the foramen magnum circumference extraction from an image. This allowed for the estimated area to be obtained. Due to the precision involved when using a vision system instead of manual efforts the area could be found to a much closer approximation than the methods that have been documented previously in the anthropological field.

Initially 2D images were tested and then using Depth from Defocus to generate the 3D images the two different methods were compared. The 3D images were expected to yield better results as the all the information required to measure the circumference would be present.

Chapter 2: *Livewire* Background and Implementation

There are a number of different techniques that have been applied in image editing. Most notably the *Magic Wand* and *Active Contours* approaches. [8] Given a user specified sample point or region, *Magic Wand* computes a region of connected pixels such that all the selected pixels fall within some adjustable tolerance of the sample statistic. In terms of algorithmic properties, it seems somewhat slow, unintelligent, and unpredictable. Drawing an approximate contour around an object initialises *Active Contours*. They are called *snakes* since the contour appears to ‘wiggle’ and ‘slide’ as it seeks a minimum energy state combining smoothness and image features. By using the result from one frame as the approximate contour in the next frame, snakes can track a moving object through a video sequence. Algorithmically, snakes are fast, robust, seemingly intelligent, and can be overridden by nudging on or pulling at portions of the snake during minimisation. The *Livewire* interactive optimal path selection tool is the technique used in this instance as the program is already been implemented within the Visions Systems Group and has distinct advantages compared to the other techniques, as it uses a dynamic programming to find the optimal boundary of an object.

2.1 Livewire

The *Livewire* program is a semi-automated procedure used for edge detection and object extraction in an image. [9] It allows for the user to interactively select the most suitable boundary, from a set of all optimal boundaries emanating from a seed point, interactive optimal 2D path selection, by applying simple gesture motions with a mouse to extract the object quickly and accurately. It entails training facilities and automatic optimal feature and transform selection methods so that these assignments that can be made with consistent effectiveness in any application.

The user first selects an initial point on the boundary. For any subsequent point indicated by the cursor, an optimal path from the initial point to the current point is found and displayed in real time. The user thus has a live wire on hand, which is moved by moving

the cursor. If the cursor goes close to the boundary, the live wire snaps onto the boundary. At this point, if the live wire describes the boundary appropriately, the user deposits the cursor, which now becomes the new starting point and the process, continues. Interactive dynamic training is employed to freeze unchanging segments and allows the user to input additional seed points, this is in case of any ambiguities in the edge of the object being extracted. A few points are usually adequate to segment the whole 2D boundary.

2.1.1 Dynamic Programming, Graph search

Livewire implements Discrete Dynamic Programming as a 2D graph-searching problem for boundary detection. The 2D dynamic programme search window is the entire image. Active points emanating from the seed propagates faster where edge magnitude local costs are lower, i.e. the optimal path. The optimal graph search is based on the Dijkstra algorithm. [9] It extends the boundary tracking method by utilising the set of edge features.

Path optimisation is formulated as a graph search algorithm that computes the minimum-cost, n-link path from seed to all other edge pixels. The Canny Edge operator is applied to extract the edges. The gradient magnitude cost feature links together the minimum cumulative cost path around the object beginning with the seed pixel. The neighbouring points of the seed pixel are then evaluated, with the diagonal local costs having been scaled by the Euclidean distance, i.e. $\sqrt{2}$. The neighbour of least cost is then expanded in the same manner with the inclusion of the original cost from the seed point to that point, the cumulative feature.

An important aspect to note is that the point currently on the active list may change if even lower cumulative costs are computed from its inactivated neighbour.

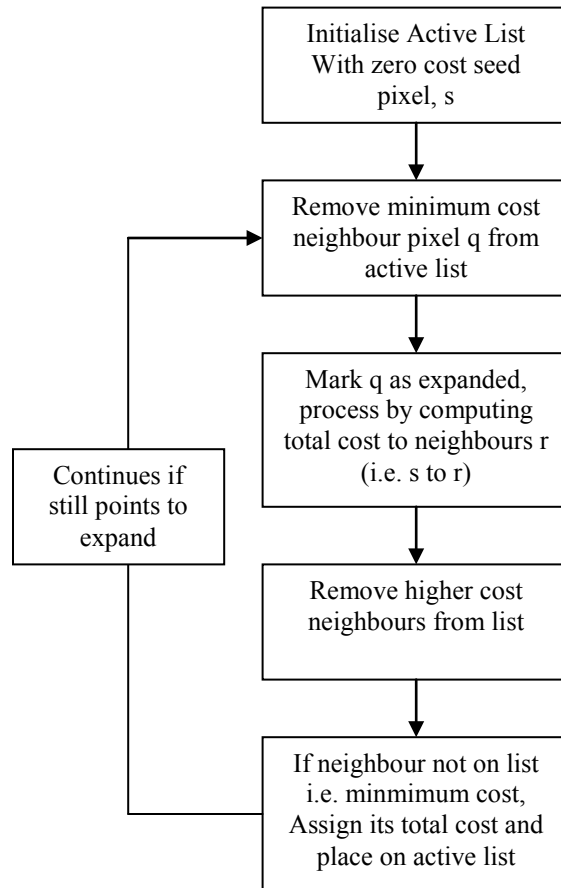


Figure 4: Flow Chart of *Livewire 2D* Dynamic Programme Graph Search Algorithm

The flow chart of Figure 4 gives a visual indication of how the algorithm updates the neighbouring pixels with respect to the cumulative costs derived from the cost function. As the process loops back it only does so if there are still points on the image to expand. It checks the cost of all the pixels that have a path to the seed point s , whether an immediate neighbour of the seed not removed from the list or a neighbour of a minimum cost cumulative path pixel. By this process it checks every possible path that emanates from the seed pixel finding the lowest ones over the iterative approach.

2.2 Overview of the Final System

Figure 5 gives an indication of the sequence of the final implementation of the system. Initially the 2D or 3D images are loaded. Then the Images area calibrated through the *livewire* extraction of the scale applied to the image detailed in Chapter 5. After calibrating the images the edge extraction is applied to the image and for the 2D case the circumference, length, width and area can be directly measured by the approach detailed in Chapter 4. The 3D case gives more information and thus the correction of viewpoint distortions can be inferred before the measurements are taken, the methods for which are detailed in the next Chapter, 3.

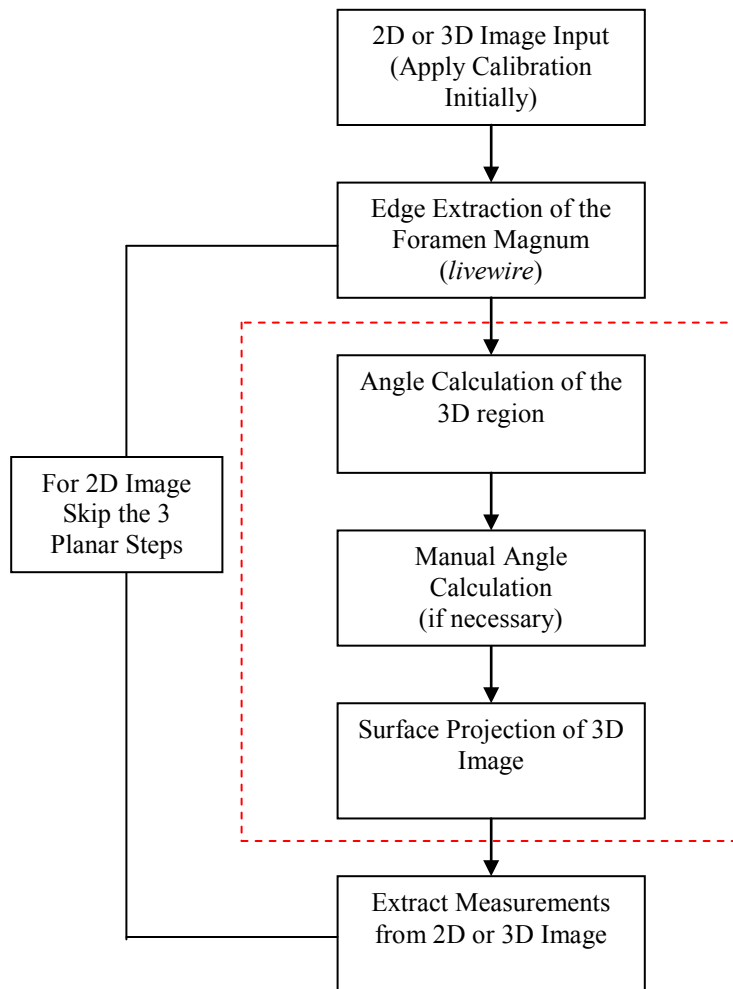


Figure 5: Flow Chart of the Vision System, red dashed box indicates exclusively 3D operations

Chapter 3: Statistical Analysis of 3D data

The 2D images could be easily obtained with use of a simple digital or analogue camera with a high enough resolution for the information to be transcribed correctly after scaling. The camera used for the project is a Sony XC77, solid state CCD camera, image resolution 512 x 512. The problem with 2D data resides in the fact that this data is very sensitive to viewpoint distortions, i.e. direction you look at the surface of interest. In 3D these distortions can compensate for by projecting the extracted planar on a planar surface perpendicular on the optical axis of the camera. Using Depth from Defocus, DFD, Least Squares Planar Fitting and Planar Projection this was achieved.

3.1 Depth from Defocus

The 3D information can be obtained using various techniques. The depth from defocus method uses maximal resemblance estimation in a scene by examining the local information. Weak textures or texture-less scenes however have inaccurate depth estimation results. The solution to this problem is to introduce a texture onto the image involving the use of a structured light. To employ a structured light a slide projector generated a symmetrical rectangular grid. The textural information supplied from the grid was organised in equally spaced lines. The depth information supplied by the depth from defocus allows 3Dscene interpretation. [10]

This structured light is interpreted by measuring the apparent blurring of the projected pattern. The resulting pattern of grey scale levels from the actively illuminated image is very spiky and thus difficult to analyse. The depth estimation should have the same pattern. The stripes would not match perfectly at the borders of the image, due to the change in distance; i.e. the depth estimation is not continuous when sudden changes in depth occur.

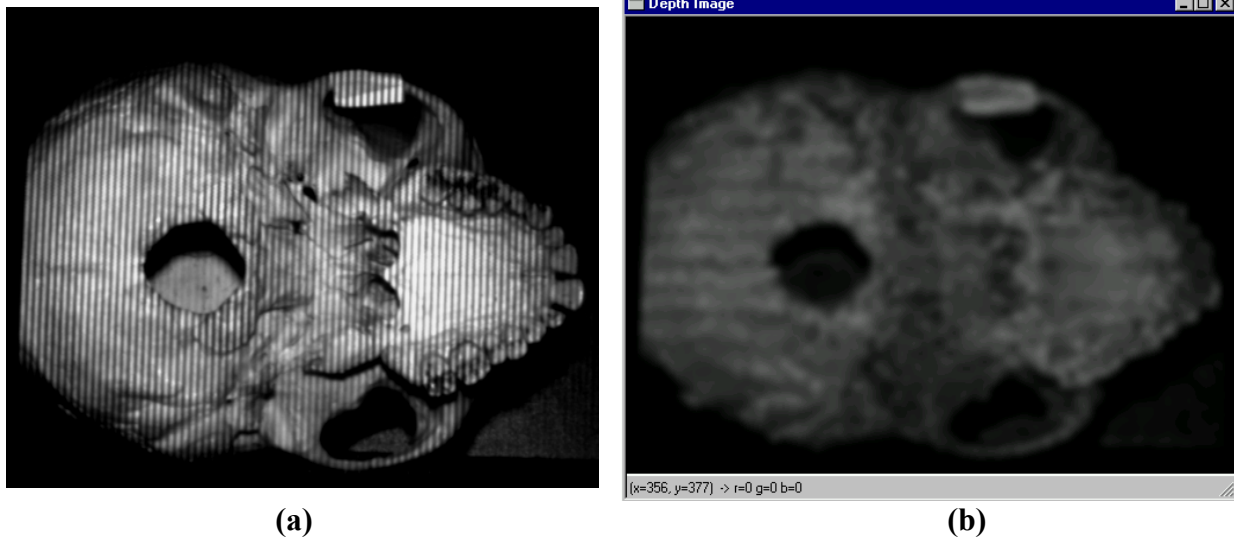


Figure 6: Actively Illuminated Image and Computed Depth Image of Skull 6

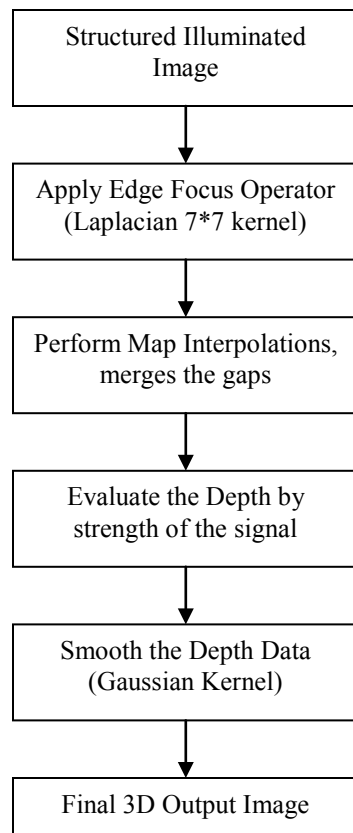


Figure 7: Flow Chart of 3D Information Computation

Figure 7 indicates the procedure used for computing the 3D information from the actively illuminated 2D image, an example of which is shown in Figure 6 (a). A Laplacian operator is applied to focus the edge information in the image. Two interpolations are performed to enhance and merge the gaps of the projected grid information. From which the strength of the signal can be obtained and represent the z plane data, becoming effectively a 3D image. Gaussian kernels of standard deviation 1.5 smooth this depth information, to give the final 3D output image of Figure 6 (b).

3.2 Statistical Analysis of 3D data - Orthographic View

The next aim is to determine the spatial orientation of the 3D image. This was achieved by using eigenspace analysis to constrain the object rotation of the z component and estimating the remaining rotations by computing the normal to the surface from the object's range of data, i.e. employing Least Square Planar Fitting. This is applied by the 3D > Orthographic view command.

3.2.1 Least Square Planar Fitting

This section summates Least Square Planar Fitting of 3D data points of the form x, y and z, where z is functionally dependent on the x and y co-ordinates. In this case the data for x and y is given by the coordinate values in the image and the z is the grey scale depth information. Least square planar fitting works on the premise that when given a set of sample data for the given set of m points the planar coefficients A, B and C can be determined. So that the sum of the squared errors between the z_i sample and the plane value $Ax_i + By_i + C$ is minimised. [11] Note the error is only measured in the z direction. The error is defined as,

$$E(A, B, C) = \sum_{i=1}^m [(Ax_i + By_i + C) - z_i]^2$$

This function is non-negative and the graph is hyper-parabolic whose vertex occurs when the gradient satisfies $\nabla E = (0,0,0)$. This leads to a system of three linear equations in A, B, C that can be solved easily.

$$(0,0,0) = \nabla E = 2 \sum_{i=1}^m [(Ax_i + By_i + C) - z_i](x_i, y_i, 1)$$

From this equation the following matrix can be inferred,

$$\begin{pmatrix} \sum_{i=1}^m x_i^2 & \sum_{i=1}^m x_i y_i & \sum_{i=1}^m x_i \\ \sum_{i=1}^m x_i y_i & \sum_{i=1}^m y_i^2 & \sum_{i=1}^m y_i \\ \sum_{i=1}^m x_i & \sum_{i=1}^m y_i & \sum_{i=1}^m 1 \end{pmatrix} * \begin{pmatrix} A \\ B \\ C \end{pmatrix} = \begin{pmatrix} \sum_{i=1}^m x_i z_i \\ \sum_{i=1}^m y_i z_i \\ \sum_{i=1}^m z_i \end{pmatrix}$$

This solution provides the least squares solution of $z = Ax + By + C$. However using a small number of points to compute the normal vector is eminently susceptible to error in depth estimation.

3.2.2 Planar Projection

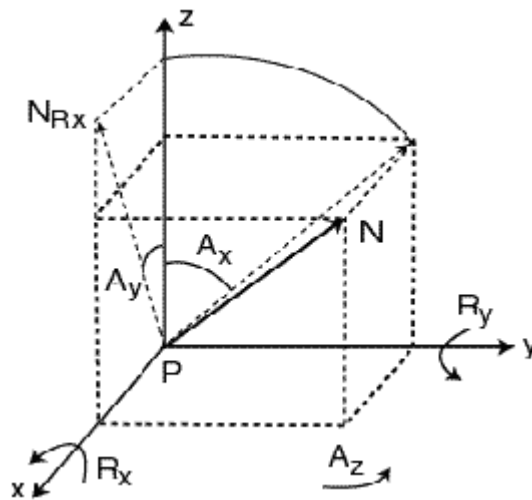


Figure 8: Rotations constrained by the normal vector N to the object surface [12]

The normal vector associated with $[x,y,z]^T$ is represented in homogeneous form as $N=[n_x,n_y,n_z,1]^T=[A,B,-1,1]^T$. The aim is to transform a plane so that the normal vector lies along the z direction of the reference frame. The image of the transformed plane can be simply formed by ignoring the z component of the transformed points. The rotation about the z-axis is estimated using Principal Component Analysis PCA analysis. [12] The desired transformation is formulated as

$$H = T_0^{-1} * R_Y * R_X * T_0$$

Where T_0 is a transformation that centres the point Q about the origin, and R_X and R_Y are rotations about the x and y-axis respectively. T_0 has the form,

$$T_0 = |I - M| \text{ where the mean vector } M = \begin{pmatrix} \frac{1}{m} \sum_{i=1}^m x_i \\ \frac{1}{m} \sum_{i=1}^m y_i \\ \frac{1}{m} \sum_{i=1}^m z_i \\ 1 \end{pmatrix} = \begin{pmatrix} m_x \\ m_y \\ m_z \\ 1 \end{pmatrix} \text{ and I is the Identity Matrix}$$

The rotations about x and y-axis have the form

$$R_X = \begin{pmatrix} 1 & 0 & 0 & 0 \\ 0 & \cos A_X & -\sin A_X & 0 \\ 0 & \sin A_X & \cos A_X & 0 \\ 0 & 0 & 0 & 1 \end{pmatrix} \text{ and } R_Y = \begin{pmatrix} \cos A_Y & 0 & \sin A_Y & 0 \\ 0 & 1 & 0 & 0 \\ -\sin A_Y & 0 & \cos A_Y & 0 \\ 0 & 0 & 0 & 1 \end{pmatrix}$$

The rotation angle about the y-axis is computed using the transform $N_{RX} = R_X N = [n_{rx}, n_{ry}, n_{rz}, 1]^T$ as A_y is $-\tan^{-1}(n_{rx}, n_{rz})$. Similarly the x-axis is rotated with respect to N_{Ry} .

Note: That when rotating about the y axis N becomes $[n_x, 0, n_z, 1]^T$ or $[A, 0, -1, 1]^T$ i.e. ignoring the y component and similarly for the x rotations N becomes $[0, n_y, n_z, 1]^T$ or $[0, B, -1, 1]^T$.

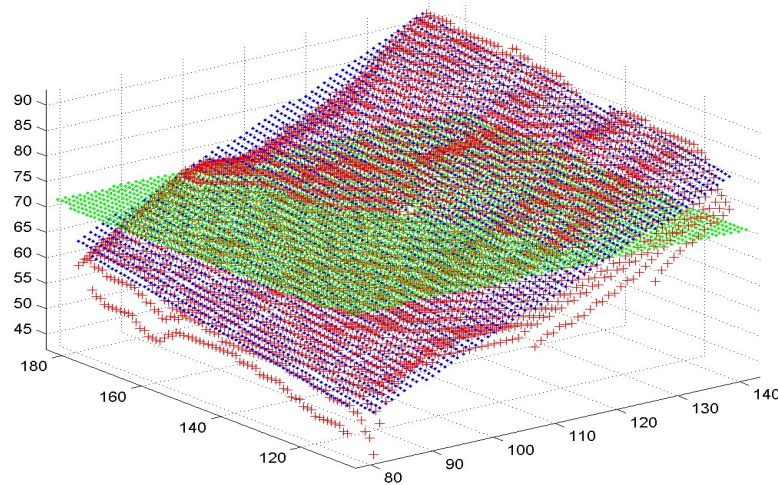


Figure 9: 3D view demonstrating Orthographic projection [12] Red-3D surface data points, Blue-Least square planar fitting of the points, Green-Transformed plane

3.3 Image Pixel Dimensions

Due the camera specifications in which the pixels were rectangular rather than square with the vertical axis being larger than the horizontal axis in the ratio 4/3. Therefore the images were elongated along the y-axis.

To achieve this the current height of the image being loaded was inferred to scale the image against the desired height or y value. The scale factor in this case was 0.75 as the y-axis of each pixel was a third greater than the x-axis. Multiplying this by the original column value gives the user specified length. Essentially each pixel is reduced or increased in the y direction and this is assigned to the new resized output image.

The program at each loading of a new image executes the dialogue box below. No entry of a resize factor will cause the document to fail to load. If the camera dimensions are equal in both directions, i.e. the pixel dimensions are square; an input of one will not induce a change in the image.

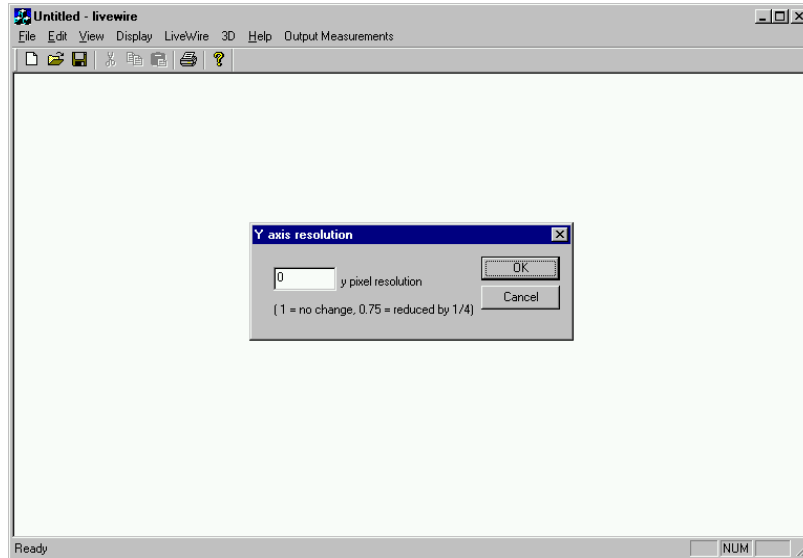


Figure 10: Image of Resizing Image Dialogue Box

Chapter 4: Measurement Code

As discussed the Livewire program was adapted to obtain the circumference of the images. Additions to the code were then made to the program so it supplied the additional measurements, along with calibration code to give the information in metric measurements.

4.1 Initial Code

Initially a separate C program for testing the approach was set up. It consisted of devising the following matrix,

$$test_matrix = \begin{vmatrix} 1 & 2 & 3 & 4 & 5 \\ 2 & 4 & 6 & 8 & 10 \\ 3 & 6 & 9 & 12 & 15 \\ 4 & 8 & 12 & 16 & 20 \\ 5 & 10 & 15 & 20 & 25 \end{vmatrix}$$

The matrix was devised to represent a set of pixels at different grey scales. As the image that is analysed will consist of varying grey scale pixels. The matrix was created by using two 'for' loops that updated the value at each coordinate of the matrix by multiplying the current row value plus 1 by the current column value plus 1. Noting that the first column and row are valued at zero i.e. value at co-ordinate 0,0 is $(0+1)*(0+1)=1$, up to the final column and final row value of four i.e. value at co-ordinate 4,4 is $(4+1)*(4+1)=25$. The program found the largest distance between coordinates that were at the value five, i.e. coordinates equal 0,4 and 4,0, and then proceeded to find the perpendicular width with the values in the range 0 to 25, i.e. coordinates equal 1,0 and 4,3.

The distance was evaluated using the Euclidean distance approach.

$$\text{Euclidean Distance} = \sqrt{(x - x_1)^2 + (y - y_1)^2}$$

The perpendicular width was found by obtaining the slope of this maximum length line using its coordinates, inverting it, changing the sign and only computing the width if the line equalled this inverted negated slope. Thus the maximum length was 5.656854 pixels, i.e. $\sqrt{(0-4)^2 + (4-0)^2}$ and the maximum width was 4.242640 pixels, i.e. $\sqrt{(1-4)^2 + (0-3)^2}$. The detection of the lines by the system were as follows, with the length highlighted by the round brackets and the width highlighted by the square brackets.

$$output_test_matrix = \begin{matrix} 1 & [2] & 3 & 4 & (5) \\ 2 & 4 & 6 & (8) & 10 \\ 3 & 6 & [(9)] & 12 & 15 \\ 4 & (8) & 12 & 16 & 20 \\ (5) & 10 & 15 & [20] & 25 \end{matrix}$$

By printing out the coordinates of each loop the progress and accuracy of the system could be monitored and the results above collated with the expected output.

4.2 2D Information Acquisition

The program was set up to work on a 2D digital image. The original skull used for testing was one that was used for teaching purposes in the anthropological department in UCD. Its top half of the skull was sawn off so that the skull lay flat on a surface. For this sample skull the contrast between the skull surface and the aperture was high. Due to the fact when laid on its side and the image was taken the light did not hit the inner surface of the skull but its rays shone through to the distant background so its illumination effects were minimal

Initially the code was added to the LiveView.cpp file in the *Livewire* program. Within the document this meant the measurements were taken once the object had been extracted. A new function 'lengthwidthperimeter' was defined within the document and called upon after the object extraction, the definition of which is discussed in the next paragraph.

However as this function was put into use one the curve surrounding the object was closed and within the criterion for the livewire extraction corresponding to the movement of the mouse it greatly increased the run time needed to output the final closed image, with the measurements included. At times taking up to forty seconds on particularly large extracted objects in the image to give the measured segmented output image, which was the case for the original sample images used. It was decided to try and apply the measure once the output image had been returned. It was discovered this also increased use-ability to the operator as the measurements could be applied as when they desired.

A Menu item, Output Measurements > 2D Measure, was added to the graphical interface. This method was applied to the segmented output image obtained by *Livewire* and the image of the 2D edge extraction was then analysed by the system. The approach was adapted from the initial test program to find the longest distance that featured in the foramen magnum, i.e. the aperture area. The extracted circumference was represented by pixels valued at 255, i.e. white, on the segmented output image. By scanning through the white pixel coordinates in the image and then finding the longest Euclidean distance to the other white coordinates in the image and thus perpendicular maximum width.

The Bresenham line function was used to apply two lines representing the length and width. This takes in the segmented image and draws a line of a defined grey scale, initially set to 200 for both, onto the image between each pair of x and y coordinates that were found to represent the maximum measurement. This was particularly useful when assessing the accuracy of the measurement acquisition.

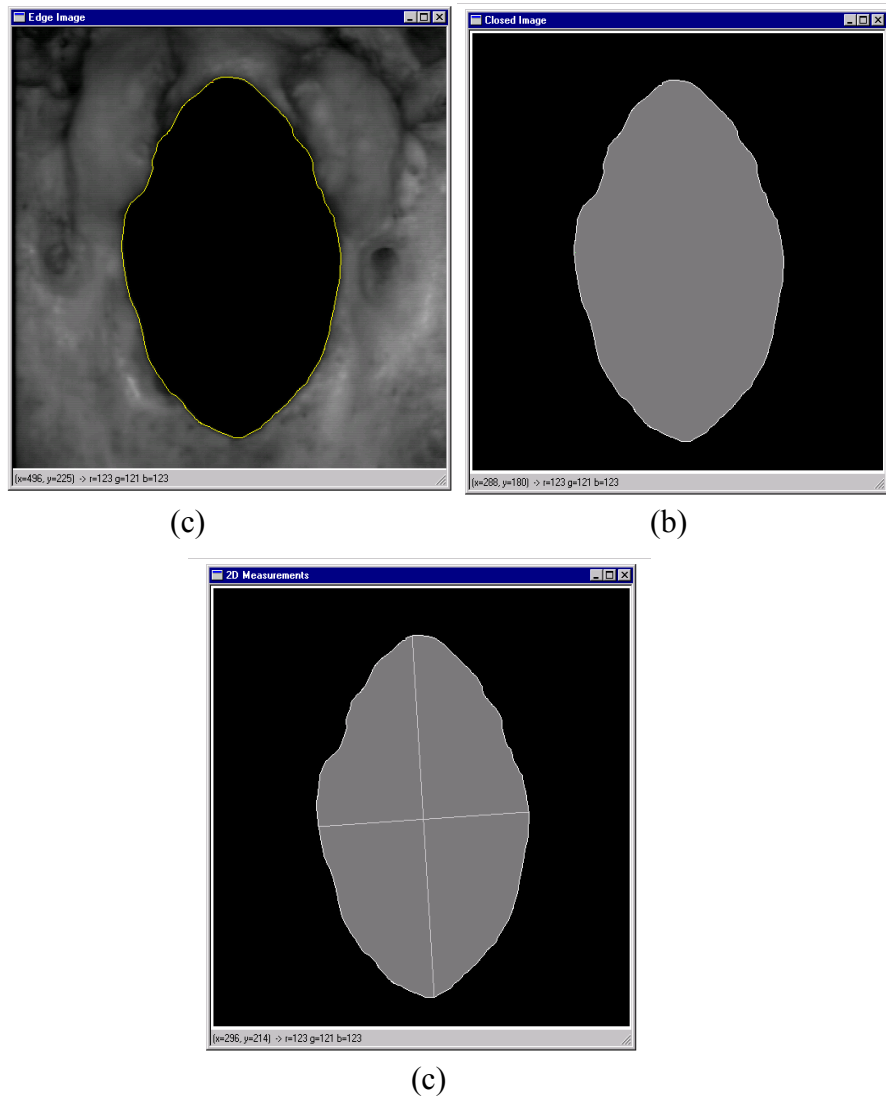


Figure 11: Initial Result Images: (a) Original image with Livewire Boundary Highlighted, (b) Output Segmented Image and (c) Test Results of 2D Measure

Note: Test Images were not Resized

The initial image results on the previous page give an indication of how the perpendicular measures outputted. Further confinements in the calculations were added later which will be discussed in the testing section of the report.

The circumference and area were obtained from image (b). As can be deduced the area was taken to include the white pixels and the approximately mid grey pixels, grey scale

value 255 and 123 respectively. Similarly the circumference required the attainment of the number of white edge pixels of the segmented image (b). The findings of all the measures at this point of testing were still in pixel format and of no relative use to an anthropologist as the scale of the image was unknown.

As the Bresenham line function could not cope with assessing a line to be drawn with no co-ordinate inputs as there was no segmented image loaded to extrapolate the results. So only if a length had been detected would the code implemented further. In other words the image being evaluated had been segmented. If a segmented image was not extracted the program would simply yield either large or zero output answers, depending on how the variables were initialised, and a blank image.

4.3 3D Range Acquisition

The 3D images were obtained by using the active Depth from Defocus technique. This meant that the method used for obtaining the circumference, length, width and estimated area of the skull for the 2D images could be easily transcribed for the 3D case. This is due to the fact the depth of the image is represented by grey scales and is in fact the equivalent of a 2D image with 3D information. This meant the segmented 3D edge image could be analysed in the same manner. An additional menu item was added to the programs files which was Output Measurements> 3D measure.

However further analysis was applied to the 3D information. As mentioned in Chapter 3 a transform could be applied to the 3D information to eliminate any viewpoint distortions, so once the 3D information was extracted the orthographic view relative to the depth information, i.e. z-axis, was extrapolated. This gave the planar projection of the x and y coordinates of the 3D edge image. Thus this information was used to deduce the planar information without any tilt factor. Simply another function was implemented in called 3D orthogonal measure, i.e menu item Output Measurements> 3D Orthogonal Measure.

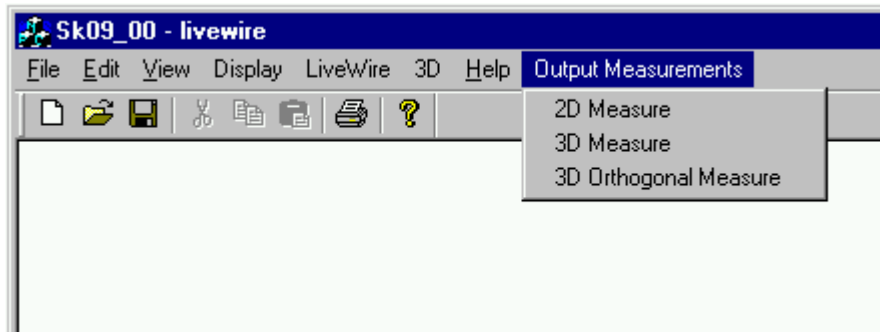


Figure 12: Graphical Interface of the Additional Measurement Functions

Chapter 5: Calibration

One of the most significant parts of this project is the calibration. It is highly important to convert the pixel level information into metric measurements that can define exactly what the extracted information is telling the user. Initially the calibration technique was to place a flat black square of known dimensions onto the surface of the skulls as close as possible to the planar surface at which the information was being extracted.

Two Calibration Images were used to test how accurate the scaling of the image was being implemented. The two images were named Calib1.bmp and Calib2.bmp. The former consisted of square compact disc label with dimensions 12cm x 12cm and the latter imaged a square object with a dark inner rectangular surface. With the exterior dimensions being 5cm x 5cm and the inner rectangular surface 3.5cm x 2.3cm. As the images were acquired with the same camera as before they were scaled to reduce each y pixel dimension by 0.25 to give square pixel dimensions as the cameras resolution elongated the image.

5.1 Scaling Factor

The interface function Scale was used to give the final output measurements in centimetres. It calculated the number of pixels that depict one centimetre. This is done with the use of Livewire edge extraction along with user input, i.e. the scaling factor, which was required by the program to evaluate the scale from the known dimensions of the square. Initially the Scale function was calculated by an approach similar to that of the foramen magnum length and width method. By finding the largest distance across the square i.e. the hypotenuse, and getting the length of the equal sides. This method gave significantly changeable values for the scale of a side due to the not always exact nature of the extraction and the skewed square image. Often up to a few of pixels in difference in the range 24 to 27 representing one centimetre for Calib1.bmp. Taking this into account the measurements could be up to 12% inaccurate. This led to the more reliable

and efficient calibration approach described below for which errors were significantly decreased.

Scale worked by counting the number of pixels within the extracted closed output image, thus giving the area in pixels of the square. The width of the square was given by finding the square root of the pixel-defined area. This output value represented the known width of the object. Finally the user defined input scale factor was asked for by the system, this allowed meant that the width was multiplied by the factor to give the pixel representation of one centimetre.

It is important to note at this point that the Scale or 2D Measure did not use the white pixels from the edge extraction for their calculations. This is significant and is discussed in the next section of this chapter, 5.2, as inclusions of these gave variance in the results.

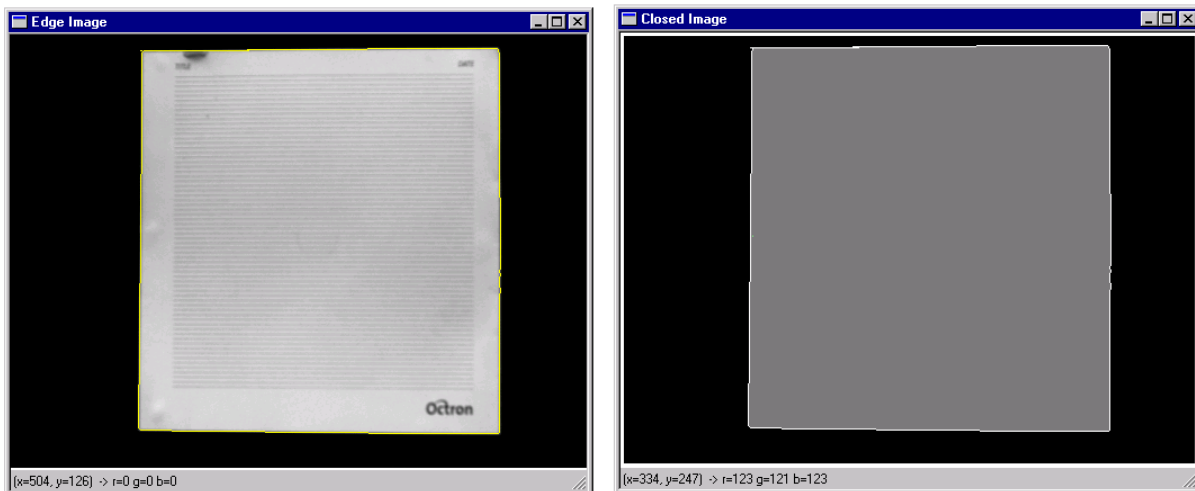


Figure 13: Calibration Image 1 (Calib1.bmp) Livewire Edge Image and Closed Output Image

For the calibration of the Calib1.bmp image the scale factor was entered in as 0.083333333, i.e. one twelfth, to give the number of pixels representing 1 cm as the edge of the square was a length of 12cm. This yielded 27.376745 pixels representing 1cm, i.e. 328.520928 equals 12cm. Applying the 2D measure to the image the outputted area yielded 143.999991cm^2 and the circumference of the square came in at 48.216105cm. Both these results were quite close to those expected the exact area ideally being 144cm^2

and the circumference being 48cm long. The slight discrepancy in the perimeter appeared to be due to the human error that occurs in the semi-automated Livewire approach.



Figure 14: Calibration Image 2 (Calib2.bmp) Livewire Edge Image and Closed Output Image

For the image Calib2.bmp the scale factor was 0.2 to give the number of pixels representing 1 cm as the edge of the square was a length of 5cm. This yielded 27.215437 pixels representing 1cm, i.e. 136.077184 equalled 5cm. Similarly applying the 2D measure to the image the outputted area yielded 24.999999cm² and the circumference of the square came in at 19.731449cm. The apparent curved edges of the outer square indicated that the scale factor would not be exact, as the area of the extrapolated edge image would be less. Evidently the area given is a good approximation as the method in obtaining it is similar to the method used to find the scale. The change in perimeter value to the expected 20cm indicates not only human error, but also the drop in the scale factor. The scale was then used to evaluate the area and perimeter of the inner rectangle that were 8.114165cm² and 11.427338cm. These compared well with the actual known values of 8.05cm² and 11.6cm.

5.2 Testing the Scale

At times *Livewire* appeared to produce an image where the lower valued pixel at the edge was highlighted to indicate the presence of that edge. As the scale did not take into account the extra white pixels it appeared to work fine with the calibrated images as their square shapes consisted of a white object on a black background and thus the approximate mid-grey pixel values took the whole object into account. This led to possible errors though when using the scale on the rectangular inner image of Calib2.bmp as this was a black area within the white 5cm*5cm region. Meaning that a layer of white pixels was in fact shaved from the total area of the shape. This would indicate that the above area would actually be slightly larger not smaller as is required for an exact match of the known and vision system obtained results.

This insinuated that when re-evaluating the code the image area should also include the white highlighted pixels as well as the mid-grey level centre pixels. Due to the fact the aperture in the skulls worked on a similar principal to the inner rectangle of the second image, i.e. the aperture being darker than the skull edges. The scale also obeyed the same principal was as mentioned taken to be a black square which lay upon the lighter surface of the skull. The next part deals with whether or not the assumption above would actually be held true when implementing the functions.

To do this the white pixels were not used when calculating the scale for Calib2.bmp but in 2D measurements for the area. 0.2 as before multiplied the 136.047786 pixels, representing the edge length of the square, to give scale of 27.209558 pixels. As the scale factor was reduced the area of the image was increased to 25.722621cm² and the perimeter of the outer square remained at a similar value 19.662209cm. However the area of the inner rectangle increased 8.528283 cm² and the perimeter increased 11.466559cm.

Another approach could also be taken with white pixels used in the scale and 2D measurements for the area. The 27.605072 pixels indicated 1 centimetre, i.e. 138.025360 * 0.2. The area was exact as expected at 24.999999 cm² were as the perimeter decreased

19.525397cm. Similarly a drop in the area and perimeter of the inner rectangle occurred with the increased scale to 8.290903 cm² and 11.374721 cm respectively.

5.2.1 Testing the Scale for the Skull Images

Another test was applied to the scale on one of the skulls, to see if this coincided with the test results of Calib2.bmp. The image of Skull 6 from the UCD collection was used. A 1.5*1.5cm square was produced by mill machine that guaranteed high accuracy, 0.0001mm degree of error. The square was used to calibrate the images so the pixel-defined width was reduced by two thirds, i.e. a floating point number of 0.666666, to give a 1cm scale.

The results were as follows and they collaborated well with the results above.

SKULL 06	PIXELS = 1.5CM	PIXELS = 1CM	AREA (CM ²)	CIRCUMFERENCE (CM)
Known Measurements			2.25	6
White included in Scale and 2D Measure	40.049969	26.699951	2.250005	5.692894
White not included in Scale and 2D Measure	38.091994	25.394636	2.250005	5.867381
White included in Scale only	39.962482	26.641627	2.034444	5.742892
White included in 2D Measure only	38.052595	25.368370	2.484639	5.952294

Table 1: Calibration Results of Skull 6

The elimination or inclusion of the white pixels alters the results when obtaining the 2D measure results and lead to the decrease and increase in area respectively. In actual fact the results above prove that the perimeter and area values are working accordingly with the scale produced. I.e. the final two scale values only decrease or increase due to the exclusion or inclusion of the white edge pixels.

It is also noteworthy that these results gave little variance over a number of executions and recalculations of the scale. At most the scale varied approximately 0.1 pixels which in relation to the results above gave changes of at most approximately 0.7%.

5.3 Final Scale

On further testing of skull number 6 it was found that when testing the results on the foramen magnum the scale inclusive of the white pixels was the best method to use. In turn the 2D measurements for area included the white pixels as they were consistently on target with the manual results previously taken. Notably if the scale is not calculated before measuring the output image will indicate where the perpendicular measurements lie but the output answers will not be defined. Thus the program gives an output of zero for each, which should indicate to the user to calibrate the system.

The scale was applied by dividing the number of pixels comprising the circumference by it. Similarly the scale divided the length and width to give an output in cm; the scale squared however divided the area to give an output in cm^2 . This scale application was then put in use for the 3D measure and 3D orthogonal measure on the graphical interface as the data is extracted in a similar fashion.

Chapter 6: Testing

The aim of the project is to devise a system that will generate reproducible results. For this reason it was important to investigate the reliability and viability of the two dimensional approach in the forensic field. Further testing of the 3D was implemented to give an idea of how any viewpoint distortions could be remedied. Five Skulls were supplied by UCD for testing, numbered 6, 9, 11, 13 and 14.

6.1 Determining Robustness

The initial testing of the program involved doing a series of tests on each image. A semi-automatic Livewire approach was applied to each image, ten times in order to find the accuracy and any possible variations that may occur when implementing the program for the length and width measures. It was found upon numerous runs that the Foramen magnum length and width coordinates remained in relatively the same position and yielded similar results. The length width results for skull nine can be seen below.

SKULL NO 9	LENGTH (mm)	X1	Y1	X2	Y2	WIDTH (mm)	X1	Y1	X2	Y2
	36.62338	196	156	289	171	33.50649	241	210	255	125
	37.10526	196	157	289	171	35.13158	237	211	251	123
	37.89474	196	156	287	188	32.76316	223	202	251	124
	37.10526	196	157	288	176	33.55263	232	206	250	123
	37.10526	196	157	289	171	33.55263	235	207	248	123
	37.10526	196	157	289	171	33.55263	232	206	256	123
	37.10526	196	157	289	171	33.55263	236	207	248	123
	37.10526	196	156	289	171	33.55263	234	207	248	123
	37.10526	196	157	286	185	32.76316	224	202	249	123
	37.10526	196	155	289	170	34.73684	233	210	247	123
Average	37.13602					33.66644				

Table 2: Length and Width Results and Coordinate Results for Skull 9

Due to the fact the application is semi-automatic the edge detection is never exactly reproduced. Slight co-ordinate differences were a result of this. As can be imagined the perimeter yielded more significant errors at times due to the fact that areas were edges were to be detected were ambiguous to the system.

Tilting the image by approximately thirty degrees with respect to the y-axis or midsagittal plane gave dubious results in the 2D images as would be expected. Due to viewpoint distortions the length reduced significantly, these being discussed further on in both 2D and 3D testing.

SKULL NO 9	LENGTH (mm)	X1	Y1	X2	Y2	WIDTH (mm)	X1	Y1	X2	Y2
	30.78947	185	166	262	172	33.94737	214	208	225	123
	31.97368	185	161	264	178	33.55263	210	206	228	123
	31.57895	185	167	264	178	34.34211	216	209	228	123
	31.97368	185	163	264	180	33.55763	210	206	228	123
	30.78947	185	162	262	177	33.15789	210	206	224	123
	31.97368	185	164	265	176	34.34211	216	209	229	123
	31.57895	185	168	264	180	33.94737	214	208	227	123
	31.97368	187	154	266	171	33.94737	211	207	229	123
	31.57895	186	159	264	175	35.13158	215	208	233	121
	31.57895	185	164	264	177	33.94737	214	208	228	123
Average	31.57895					33.99684				

Table 3: Length and Width Results and Coordinate Results for Skull 9 tilted by 30degrees

Checking the robustness of the measures at this point did yield the fact however that the results that were acquired although fairly robust in technique, slight rotations on the results when compared to the midsagittal plane meant the length and hence width of the foramen magnum were badly defined. As can be seen from Table 2 the final average results of the image at approximately 0 degrees were 37.13602 mm and 33.66644 mm for the length and width respectively. Compared with the desired results for Skull 9 mm of 34.43 and 30.43 mm they indicate relatively inaccurate estimation.

The other measurements compared in relatively the same manner as skull 9 the results of which are shown in the figure on the next page, these results are an average of ten executions of the *Livewire* edge extraction with no significant angle,

SKULL NO	AVERAGE 2D LENGTH(LFM) IN MM	AVERAGE 2D WIDTH(WFM) IN MM	AVERAGE 3D LENGTH(LFM) IN MM	AVERAGE 3D WIDTH(WFM) IN MM
6	33.405 (33.41)	28.83 (26.13)	32.2125	28.65
11	37.27173 (35.72)	38.62038 (33.93)	38.28947	36.55263
13	40.21712 (36.07)	35.59524 (30.63)	37.33784	32.71622
14	36.96154 (36.48)	31.61539 (28.74)	36.4557	3

Table 4: Averaged Length and Width Results for Skulls 6, 11, 13 and 14

Note: the brackets indicate the measurements that have been already taken manually for comparisons.

6.1.1 Slope Constraints

The slope comparisons when applied to the test image were initially in integer format, as the coordinates of the distances were declared as integers. The approximations were good but if the slope of the maximum length was zero, the width approximation would not lie perpendicular to the length. By computing and comparing the slopes as double, i.e. to 6 decimal places, the accuracy increased but by too much, as the width slope had to be very specific and thus the widest length detected was no where near it was expected visually. As only a few possible coordinate would satisfy the negated inverted slope criterion. It was finally decided to introduce a factor of 100 to the slopes and then applying a double to integer conversion. This effectively cut off the rest of the slope information after two decimal places. The accuracy was sufficient to yield good approximations.

6.1.2 Robustness with respect to the Midsagittal Plane

Ideally the length of the foramen magnum should be relatively close to the manual results as where it is determined is specific. Were as the width results may be slightly more ambiguous when comparing, as there is a higher degree of accuracy when finding the width perpendicular to the length. As mentioned the length of the foramen magnum is actually placed on the midsagittal plane that bisects the skull in half, so the problem with this approximate lay in the fact there was no constraints on where the length would be detected. Initially when testing with the input image of the test skull did not appear to be effected by this, as the foramen magnum aperture was fairly elliptical in shape. Not until further testing of numerous skulls did it become apparent that the shape of the aperture could become more significantly circular and the slopes of the measures where slightly inaccurate in comparison with the midsagittal plane.

To counteract these effects a confinement to how the program detected its length was required. A constraint could be applied along whichever image axis the midsagittal plane lay parallel to, for these test images it was the along the x-axis. Little or no change in the y-axis coordinates of the length indicates the length is parallel to the x-axis. So initially the maximum length was only detected where no change in the y coordinates, i.e. $y1(j) - y2(m) = 0$, this was too constrictive when tested on the images. The line of code applying this is highlighted in yellow below.

```

for(i=4;i<OrigImage.Row-4;i++)
for(int j=4;j<OrigImage.Col-4;j++)
if(img2D[i+j*OrigImage.Row] == 255)
{
    for(int k=4;k<OrigImage.Row-4;k++)
    for(int m=4;m<OrigImage.Col-4;m++)
    if(img2D[k+m*OrigImage.Row] ==255) //equal white in image
    {
        length2D = sqrt(((i-k)*(i-k))+((j-m)*(j-m)));
        if(abs((double)j-(double)m)<=0) //(int)((OrigImage.Col)/100)
        {
            if(length2D>maxlength2D)
            {
                maxlength2D = length2D;maxi2D=i;maxj2D=j;maxk2D=k;maxm2D=m;
            }
        }
        length2D = 0;
    }
}

```

Allowing an increase in the difference between y2 and y1 decreased the restriction. A number of tests were applied incrementing the absolute difference by one each time. This implied that difference of the coordinates could lie between +/-1 pixel, +/-2 pixels etc. This was done for each image as alterations may have changed significantly.

The images were rotated by 90 degrees to see if the width was constrained to be parallel to the x-axis and thus detected first, would it bear a different output length of the foramen magnum. The images were resized and rotated by 90 degrees in Microsoft Photo Editor.

+/-1PIXELS	SCALE (No. Pixels = 1cm)	ORIGINAL IMAGE		90 ⁰ ROTATED IMAGE	
		LFM (mm) to y-axis	WFM (mm)	LFM (mm) to x-axis	WFM (mm)
Skull no 6	27.688717	33.22653	27.448	33.22653	27.80916
Skull no 9	26.699951	34.83152	31.83526	34.83152	31.46073
Skull no 11	26.824505	36.90655	36.16097	36.90655	36.16097
Skull no 13	26.136367	37.49565	34.05217	37.49565	34.81739
Skull no 14	27.616391	34.39986	29.33041	34.76196	29.33041

Table 5: Detecting LFM and WFM with 1 pixel difference between axis coordinates

Note: some of the results are slighted different when rotated due to slight glitches in the extraction rather than specific changes in the measurements due to rotation.

The manual values for skull 11 and 13 in particular do not match well as the skulls are slightly rotated in the image with respect to the midsagittal plane, up to 20 degrees when analysing the images. The plane lay approximately parallel to the x-axis in the other images indicated by the preferred results.

+/-2PIXELS	SCALE (No. Pixels = 1cm)	ORIGINAL IMAGE		90 ⁰ ROTATED IMAGE	
		LFM (mm) to x-axis	WFM (mm)	LFM (mm) to y-axis	WFM (mm)
Skull no 6	27.656596	32.90354	27.477988	32.90354	27.477988
Skull no 9	26.633285	34.91871	31.53948	34.91871	31.53948
Skull no 11	26.882432	36.82702	36.08304	36.82702	36.35503
Skull no 13	26.051204	37.61822	34.16349	37.23436	34.54735
Skull no 14	27.712784	34.28021	29.22839	34.28021	29.22839

Table 6: Detecting LFM and WFM with 2 pixel difference between axis coordinates

+/-3PIXELS	SCALE (No. Pixels = 1cm)	ORIGINAL IMAGE		90 ⁰ ROTATED IMAGE	
		LFM (mm) to x-axis	WFM (mm)	LFM (mm) to y-axis	WFM (mm)
Skull no 6	27.672661	32.88444	27.46393	32.88444	27.82530
Skull no 9	26.649967	34.89685	31.89497	34.89685	31.89497
Skull no 11	26.783051	36.96367	36.21693	36.96367	36.21693
Skull no 13	26.068259	37.59361	34.52474	37.59361	34.52474
Skull no 14	27.624437	34.75184	29.32186	34.75184	29.32186

Table 7: Detecting LFM and WFM with 3 pixel difference between axis coordinates

+/-4PIXELS	SCALE (No. Pixels = 1cm)	ORIGINAL IMAGE		90 ⁰ ROTATED IMAGE	
		LFM (mm) to x-axis	WFM (mm)	LFM (mm) to y-axis	WFM (mm)
Skull no 6	27.664630	32.89399	27.11043	32.89399	27.11043
Skull no 9	26.633285	34.91871	31.91495	34.91871	31.91495
Skull no 11	26.932788	36.89516	35.77712	36.89516	35.77712
Skull no 13	26.102335	37.54453	34.09657	37.54453	34.09657
Skull no 14	27.712784	34.28021	29.22839	34.28021	29.22839

Table 8: Detecting LFM and WFM with 4 pixel difference between axis coordinates

+/-5PIXELS	SCALE (No. Pixels = 1cm)	ORIGINAL IMAGE		90 ⁰ ROTATED IMAGE	
		LFM (mm) to x-axis	WFM (mm)	LFM (mm) to y-axis	WFM (mm)
Skull no 6	27.640521	32.92268	27.13408	32.89399	27.49586
Skull no 9	26.616592	34.94061	31.93497	34.94061	31.93497
Skull no 11	26.824505	36.90655	36.16097	36.90655	36.16097
Skull no 13	26.068259	37.59361	34.14114	37.59361	34.14114
Skull no 14	27.656596	34.34985	28.92619	34.34985	29.037250

Table 9: Detecting LFM and WFM with 5 pixel difference between axis coordinates

The alignment of the LFM with either axis bore practically no difference on the maximum LFM detected. They did not vary when approximated to the nearest millimetre. A constraint of a percentage of the height of the image, 512 pixels, was entered at a +/-1%. This was deduced from the +/-5 pixel restraint on the detected length, with respect to the axis its parallel to, that gave little deviation in results but enough to counteract small rotations. Choosing the constraint with respect to the resolution of the camera meant that the deviation would be in proportion to the dimensions of the image loaded. If the image specifically extracted the occipital region, rather than the whole skull as in the test images, the restraint would be minimal.

Another approach was tried by writing the code for condyles in which the slope of a line equidistant from each of them would determine the slope for the length. This however was tricky and the program ran out of memory. The idea of the approach was to take the 20 minimum y values along the upper most condyle and then take the 20 maximum y values along the lower condyle. Ranging a set of x coordinates from 0 to 20 to put the y coordinates into 2D. The idea then was to use the average value between each coordinate to then help determine the slope of the line. Due to the unsymmetrical nature of the condyles and mutations however these mean distances may not lead to good slope results

on further consideration. The code is appended onto the livewireDoc.cpp file though is inactivated.

6.2 2D Image Testing

This section deals with applying the extraction and calibration to the 2D images to obtain the desired measurements. 2D images with viewpoint distortions were also examined to display the shortcomings of 2D analysis.

SKULL NO 6	LFM (mm)	WFM (mm)	FMC (mm)	FMA (mm ²) Estimated	FMA (mm ²) Actual	SCALE
Manual Results	33.41	26.13	86	588.55		
No Tilt	32.86537	27.80916	86.6779	597.87	651.6535	27.68872
Tilted by 30 ⁰	30.33727	27.08685	79.09359	497.82	588.2621	

Table 10: Skull 6 2D Result

Looking at the results for Skull 6 in the table above it can be seen that as the estimated area of the aperture defined by the area of the circle depends completely on the extracted circumference, the results differ slightly to the manually estimated measures. Bad edge detection by the user can greatly effect these particular outputs. Often causing spikes in the output segmented image that will significantly increase the circumference and hence the estimated area. However the better approximation of the area which involves estimating the area by counting the number of pixels that comprise the segmented image divided by the scale squared was less likely to differ dramatically when the circumference was badly extracted.

The testing of the tilted images produced notable changed results. As the tilt was along the x-axis of the image, this lay in conjunction with where the length of the foramen would be measured so the length was particularly skewed. The results for the remaining skulls are tabulated on the next page. As mentioned skull 11 and 13 were rotated significantly in the associated images and therefore the comparisons with the manual

results do not relate well. This would be simply remedied by acquiring the images again with more significance made on the alignment with the midsagittal plane.

SKULL NO 9	LFM (mm)	WFM (mm)	FMC (mm)	FMA (mm ²) Estimated	FMA (mm ²) Actual	SCALE
Manual Results	34.43	30.43	95.75	729.57		
No Tilt	34.83152	31.46073	96.62939	743.03	807.8415	26.61659
Tilted by 30 ⁰	30.4226	31.17378	91.26781	662.87	709.2805	

Table 11: Skull 9 2D Results

SKULL NO 11	LFM (mm)	WFM (mm)	FMC (mm)	FMA (mm ²) Estimated	FMA (mm ²) Actual	SCALE
Manual Results	35.72	33.93	104.69	872.17		
No Tilt	36.88378	36.13865	107.2983	916.17	1019.928	26.84107
Tilted by 30 ⁰	34.27583	35.76609	102.5336	844.74	947.7626	

Table 12: Skull 11 2D Results

SKULL NO 13	LFM (mm)	WFM (mm)	FMC (mm)	FMA (mm ²) Estimated	FMA (mm ²) Actual	SCALE
Manual Results	36.07	30.63	98.74	775.85		
No Tilt	37.52007	34.07435	105.2859	882.13	930.0508	26.11936
Tilted by 30 ⁰	34.07435	32.54291	97.62874	758.4825	807.2167	

Table 13: Skull 13 2D Results

SKULL NO 14	LFM (mm)	WFM (mm)	FMC (mm)	FMA (mm ²) Estimated	FMA (mm ²) Actual	SCALE
Manual Results	36.48	28.74	94.02	703.45		
No Tilt	34.74172	28.95144	92.6446	683.02	755.0219	27.63248
Tilted by 30 ⁰	34.37983	28.95144	92.2827	677.69	709.0527	

Table 14: Skull 14 2D Results

6.3 3D Image Testing

The analysis was then applied to the 3D data images using the same scale that was acquired for each skull in the 2D case. The 3D images i.e. 2D images with grid illumination, were computed using 3D>Compute 3D in the *Livewire* program.

The least square planar fitting for extracting the angle required for correct planar projection was relatively poorly recovered on initial testing of the 3D images. To implement correct planar projection the planar coefficients were overwritten to {0.6,0,0} for {a,b,c} this indicates a 30 degree projection is required. To do this a dialogue box was added in the orthographic view function. This was implemented after the planar fitting and the user defined tilt factor could be entered. If the user did not want to overwrite the calculated coefficients it was only necessary to CANCEL the pop-up box and the orthographic view implemented as normal.

The projection was also applied to the images that were not tilted, as there is always a degree of human error. The angles outputted by the program indicated the images were slightly tilted by 1 or 2 degrees, although skulls 6 and 13 had slightly higher angles of about 3 or 4 degrees.

SKULL NO 6	LFM (mm)	WFM (mm)	FMC (mm)	FMA (mm ²) Estimated	FMA (mm ²) Actual	SCALE
Manual Results	33.41	26.13	86	588.55		
No Tilt	30.69842	26.36453	83.06633	549.09	615.6535	27.68872
Orthogonal View	31.0598	26.72569	87.03906	602.86	600.7839	
Tilted by 30 ⁰	27.448	26.00337	76.92664	470.92	544.8272	
Orthogonal View	31.7819	2.636453	84.51096	568.35	601.436	

Table 15: Skull 6 3D Results

SKULL NO 9	LFM (mm)	WFM (mm)	FMC (mm)	FMA (mm ²) Estimated	FMA (mm ²) Actual	SCALE
Manual Results	34.43	30.43	95.75	729.57		
No Tilt	33.8135	31.55926	92.42355	679.76	788.4897	26.61659
Orthogonal View	34.1892	31.93497	93.17496	690.86	769.575	
Tilted by 30 ⁰	31.17378	30.4226	97.88752	614.67	696.4435	
Orthogonal View	36.43201	30.04702	95.39928	724.24	771.3496	

Table 16: Skull 9 3D Results

Note the results for the orthographic view are slightly exaggerated for the images tilted by 30 degrees as they were tilted by a simple ‘guestimation’ using a protractor. The 30 degrees orientation is just appreciative. Thus the images tilt factor is ambiguous and by forcing the planar coefficients to imply a 30⁰ planar projection about the z-axis may cause distortions as the angle may not have been this large in the image. This is particularly notable in the results for Skull 9. However the results do indicate that the images projected to give more accurate results.

The validity of this approach is debatable however, as the user may not know the angle of the tilt and thus it would be preferable that the planar coefficients and projection were correctly formulated within the program. Instead of the approach of the user forcing the projection angle. As mentioned in the statistical analysis explanation the number coefficients cause problems in the angle estimation. The tilt angle is relatively poorly recovered due to the fact that the errors in depth estimation around depth discontinuities are significant and the number of points employed to estimate the planar is small. The improved result for skull 11 and 13 are only an indication of this and do not actually infer that the 3D method used up to this point is better. Ways in which to improve the depth estimation is discussed in section 6.3.1.

SKULL NO 11	LFM (mm)	WFM (mm)	FMC (mm)	FMA (mm ²) Estimated	FMA (mm ²) Actual	SCALE
Manual Results	35.72	33.93	104.69	872.17		
No Tilt	36.13865	33.53071	99.84699	793.34	922.6268	26.84107
Orthogonal View	36.51121	33.90327	106.1806	897.18	901.6675	
Tilted by 30 ⁰	32.41302	33.90327	91.27804	663.01	811.3064	
Orthogonal View	37.6289	32.78558	99.47443	787.43	904.86	

Table 17: Skull 11 3D Results

SKULL NO 13	LFM (mm)	WFM (mm)	FMC (mm)	FMA (mm ²) Estimated	FMA (mm ²) Actual	SCALE
Manual Results	36.07	30.63	98.74	775.85		
No Tilt	35.22292	30.62863	90.7373	655.18	787.2818	26.11936
Orthogonal View	36.37149	30.62863	93.03445	688.78	788.8942	
Tilted by 30 ⁰	34.84006	30.62863	94.56588	711.64	800.7671	
Orthogonal View	40.58293	31.01148	100.6916	806.82	891.2071	

Table 18: Skull 13 3D Results

SKULL NO 14	LFM (mm)	WFM (mm)	FMC (mm)	FMA (mm ²) Estimated	FMA (mm ²) Actual	SCALE
Manual Results	36.48	28.74	94.02	703.45		
No Tilt	34.74172	28.58954	89.38756	635.35	722.2803	27.63248
Orthogonal View	35.10362	29.31333	90.47324	651.37	703.4211	
Tilted by 30 ⁰	30.0399	28.58954	86.49242	595.31	641.7359	
Orthogonal View	35.46551	28.58954	94.81595	715.41	711.1482	

Table 19: Skull 14 3D Results

6.3.1 Varying the angle of Projection

As the 3D results from the rectified tilted images were still inaccurate, further testing was applied to the 3D images by applying varying degrees of planar projection. Different degrees for the projection were applied. The angles that generated the best results for each image are indicated in Table 20. As can be seen the angle varied significantly for each.

SKULL NO	ANGLE	LFM (mm)	WFM (mm)	FMC (mm)	FMA (mm ²) Estimated	FMA (mm ²) Actual	SCALE
6 (Manual)	-34.992	33.23617 (33.41)	26.37217 (26.13)	85.98051 (86)	588.29 (588.55)	628.5396	27.68069
9 (Manual)	-28.8108	34.91871 (34.43)	29.28666 (30.43)	96.61203 (95.75)	735.23 (729.57)	745.6313	26.63329
11 (Manual)	-24.23	36.08304 (35.72)	32.73513 (33.93)	102.2297 (104.69)	832.7572 (872.17)	832.7508	26.88243
13 (Manual)	-16.70	36.38335 (36.07)	30.63861 (30.63)	94.5967 (98.74)	712.1018 (775.85)	795.5688	26.11085
14 (Manual)	-33.0239	36.06357 (36.48)	28.12958 (28.74)	94.84718 (94.02)	715.8779 (703.45)	715.7096	27.72882

Table 20: Results from Best Angle for Projection for each Tilted Image

There were still notable differences however the results do indicate how the 3D data has the capacity for extracting the data required by projecting the image. Skull No 13 in particular had a very low circumference measurement, in fact the angle at 30⁰ yielded a better value of 96.12863mm but the LFM and WFM were inaccurate at 40.59615mm and 31.02159mm respectively.

The information is still somewhat inaccurate due to depth estimation errors. There are a number of approaches that would improve the depth estimation calculated by *livewire*. The most obvious strategy would be to use a more powerful light projector to compensate

for the drop in signal strength in areas with dark colours or a light projector with a lens with a smaller depth of field. Also a camera with a higher resolution would improve the estimation, as the images would be sharper. Using a better quality range sensor, i.e. stereo or triangulation-based laser scanners would also improve the results of the system.

6.4 Gender Identification

The gender of each of the skulls has not actually been officially determined. These samples are used for test purposes by the UCD forensic anthropology department. Nevertheless Dr Jason Last did indicate did give an indication of what he as a forensic anthropologist would believe the gender of each sample to be, by taking into account other more obviously gender identifiable features of the skull. Normally three or more anthropologists apply these methods for identification and thus they would collaborate their results.

SKULL NO	GENDER
6	Female
9	Male
11	Male
13	Male
14	Female

Table 21: Anthropologists Gender Identification of the Skulls, with approx 90% accuracy

6.4.1 Analysis of 2D Results for Identification

The results had noticeable significance, both manually and experimentally. Generally the female skulls had more elliptical foramen magnum with the male being closer to a circular shape. This is realised in the differences between the length and width. The length is significant larger then the width for females. The area however both the estimated and the more accurate findings were particular notable. As the female samples

appeared have a smaller area than the male, though skull 9 may be particularly dubious if going on area alone. As it bears the elliptical qualities substantially both qualities may be used to infer its gender. Both of these findings have been drawn attention to by previous authors in medicine and forensics as indicated in the Teixeira paper [7]. Plots of the results of the table above exhibit these assumptions more clearly, giving an indication of how the gender could be distinguished.

SKULL NO	LFM (mm)	WFM (mm)	FMC (mm)	FMA (mm ²) Estimated	FMA (mm ²) Actual
6 (Manual)	32.86537 (33.41)	27.80916 (26.13)	86.6779 (86)	597.87 (588.55)	651.6535
9 (Manual)	34.83152 (34.43)	31.46073 (30.43)	96.62939 (95.75)	743.03 (729.57)	807.8415
11 (Manual)	36.88378 (35.72)	36.13865 (33.93)	107.2983 (104.69)	916.17 (872.17)	1019.928
13 (Manual)	37.52007 (36.07)	34.07435 (30.63)	105.2859 (98.74)	882.13 (775.85)	930.0508
14 (Manual)	34.74172 (36.48)	28.95144 (28.74)	92.6446 (94.02)	683.02 (703.45)	755.0219

Table 22: Final 2D Results, Noting 11 and 13 has rotational errors

Plotting the length and width against the circumference indicates that the difference in length and width may be directly related to gender, see Figure 15. Also the circumference increases in the male skulls, as the distances become closer, i.e. the foramen magnum is more circular. Skull 9, which is considered male, is less distinguishable by these results as the circumference is smaller at 96.62939, although it does exhibit more similar length and width distances.

Skull 11 and 13 had slightly increased length and width results when compared with the manual results due to rotational effects. There was a notable variance in the length and width in Skull 13 but when referenced with the circumference the graph would have yielded the results for 13 in a similar position to Figure 15.

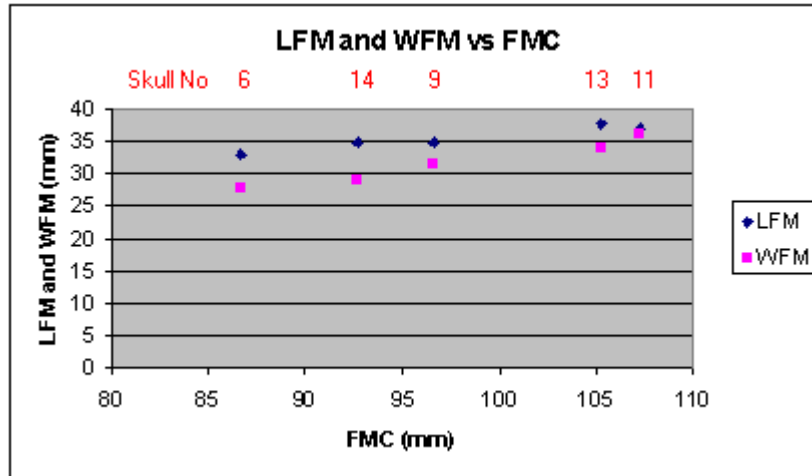


Figure 15: 2D Results, LFM and WFM vs FMC

The plot in Figure 16 displays that the male samples exhibit larger areas. Similarly the area of skull 9, both the circle-based estimation and the more accurate result, sways the results closer to the female classification. Cross Referencing the data from the two plots may allow for sex determination to be more accurate.

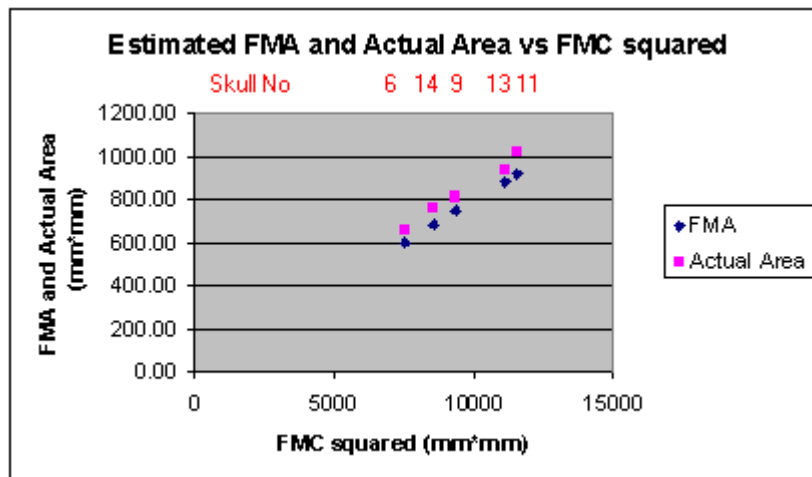


Figure 16: 2D Results, Estimated FMA and Actual Area vs FMC²

6.4.2 Analysis of 3D Results for Identification

Similarly the 3D data was examined. The results were less conclusive than the 2D data, which was explained in the previous testing section, 6.3. There are still indications of larger areas and more circularity with male samples. The difference in length and width in Skull 6 has the greatest change from the 2D results. As can be seen from Figures 17 and 18 errors in depth estimation have significantly altered the results for Skull 13. The circumference in particular has greatly reduced.

SKULL NO	LFM (mm)	WFM (mm)	FMC (mm)	FMA (mm ²) Estimated	FMA (mm ²) Actual
6	30.69842	26.36453	83.06633	549.09	615.6535
9	33.8135	31.55926	92.42355	679.76	788.4897
11	36.13865	33.53071	99.84699	793.34	922.6268
13	35.22292	30.62863	90.7373	655.18	787.2818
14	34.74172	28.58954	89.38756	635.35	722.2803

Table 23: Final 3D Results with No Orthographic View applied and Depth Estimation Errors

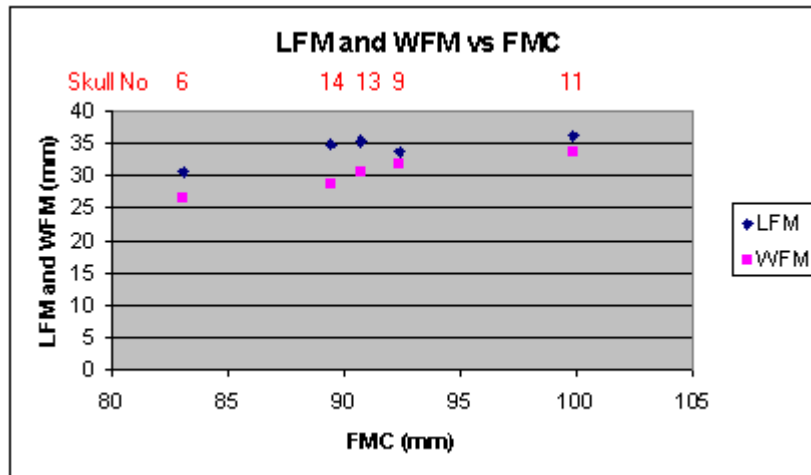


Figure 17: 3D Results, LFM and WFM vs FMC

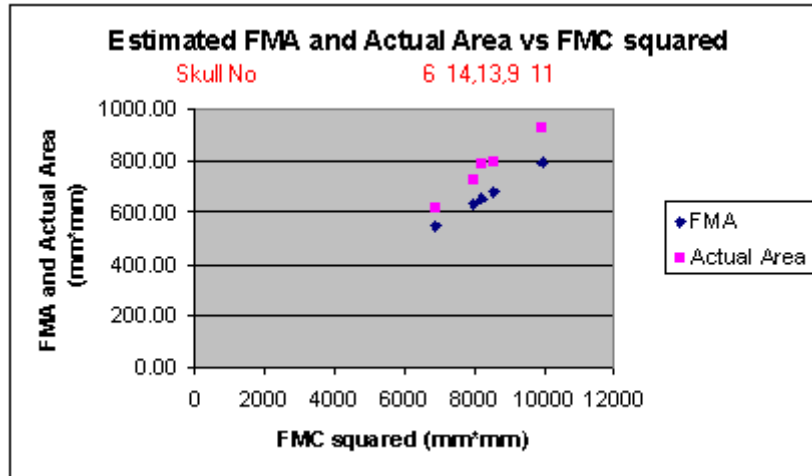


Figure 18: 3D Results, Estimated FMA and Actual Area vs FMC²

The forced tilt results from Table 20 were plotted likewise, displayed in Figures 19 and 20. To give an indication of the ‘best’ 3D results recovered. As previously indicated Skull 13 circumference recovery is notably much less than its manual value of 98.74, although the length and width measurements are ideal.

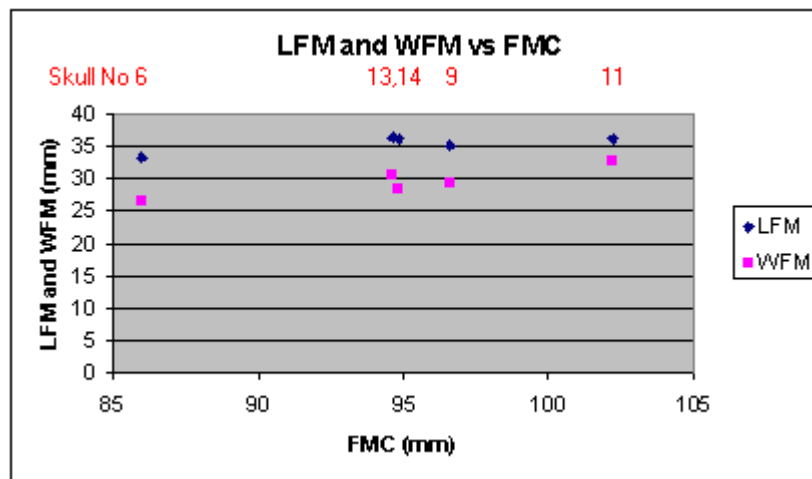


Figure 19: Projected 3D Results, LFM and WFM vs FMC

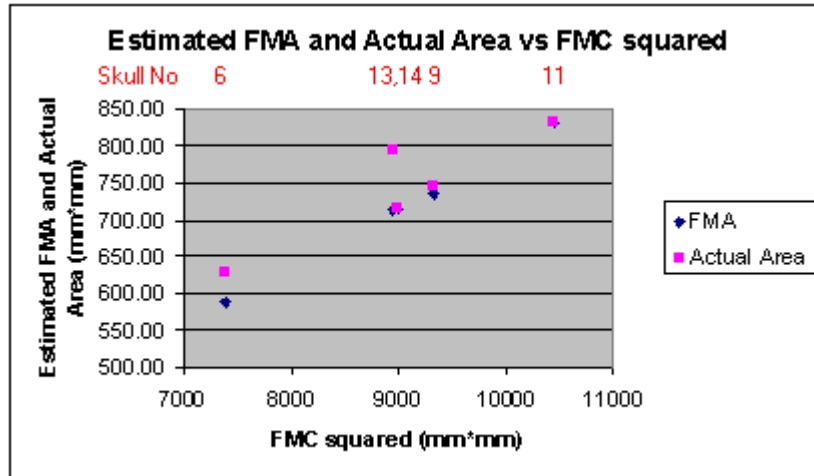


Figure 20: Projected 3D Results, Estimated FMA and Actual Area vs FMC²

With the exception of Skull 13 the 3D images yield good results and show the greater possibilities involved with 3D imaging. However for the task in hand and with the methods applied the 2D approach gave sufficiently accurate results. There are many enhancements that could be inferred to obtaining the 3D range of data that would make the 3D approach ultimately the best.

7 Conclusion

The 2D approximate is more accurate when compared with the 3D results, however as indicated, improvements could be made in the 3D images. Another advantage to the 2D approach is that it is easier to reproduce the data because of the equipment involved. The only equipment required would be a sufficiently high-resolution digital camera to obtain the images and a PC to run *livewire*. The tilt factor that may be a problem could be dealt with by employing a spirit level to gauge that no tilt exists when acquiring an image of a skull.

The most significant finding however is that the image processing allows for a fairly accurate generation of the area of the skull. The approach discussed in Chapter 1 is estimated on the basis of an area of a circle and is a very crude appraisal. This finding should bear significance in future anthropological endeavours.

Further work could include appraising how circular or elliptical the foramen magnum is. The deviations from each shape may help determine the gender accurately. An improved method in the determination of the midsagittal plane could also be applied by determining the best bisecting line of the foramen magnum into 'equal' halves.

The analysis of the findings is purely conjecture and a larger range of skulls would be required to examine fully the possible traits exhibited by either sex in this region of the skull. It would enable statistical examination of how valid these presumptions may be and note the error that may occur when testing dubious samples. This examination alone does not validate the accuracy of the identification, only presents a system that may help in future analysis of larger homogeneous sample groups.

References

- [1] An Overview of Forensic Anthropology,
Jessica Kiefer
<http://serendip.brynmawr.edu/biology/b103/f01/web1/kiefer.html>
- [2] Gender Practices of Artificial Cranial Deformation
<http://ehlt.flinders.edu.au/archaeology/gender/1998/OWEN/ESSAY.HTM#ref>
- [3] Diagram Showing Anthropometric landmarks,
Aiello and Dean 1990,
<http://mac-huwis.lut.ac.uk/~wis/lectures/evolutionary-anatomy/The%20Skull.pdf>
- [4] Robust Midsagittal Plane Extraction from Normal and Pathological 3-D
Neuroradiology Images
Yanxi Liu*, *Member, IEEE*, Robert T. Collins, *Member, IEEE*, and William E. Rothfus
- [5] Sex Determination of Fragmentary Crania by Analysis of the Cranial Base
Thomas Dean Holland, *American Journal of physical Anthropology* 70:203-208 (1986)
- [6] ‘Anomalies of Occipital Bone at Foramen Magnum (Occipital Condyles)’
Illustrated Encyclopedia of Human Anatomic Variation: Opus V: Skeletal Systems
Ronald A. Bergman, PhD, Adel K. Afifi, MD, MS and Ryosuke Miyauchi, MD
- [7] Sex Identification utilizing the size of the Foramen Magnum
W.R.G. Teixeira, M.D., Ph.D., *American Journal of Forensic Medicine and Pathology*, Volume 3
No 3 (1982)
- [8] Vision-Assisted Image Editing,
Eric N. Mortensen Brigham Young University

- [9] Intelligent Scissors for Image Composition,
Eric N. Mortensen and William A. Barrett
- [10] A video-rate range sensor based on depth from defocus
Ovidiu Ghita, Paul F. Whelan, Optics and Laser Technology Volume: 33, Issue: 3, April, 2001
- [11] Least Squares Fitting of Data,
David Eberly, Magic Software, Inc., <http://www.magic-software.com>
- [12] Pose Estimation for objects with planar surfaces using eigenimage and range data analysis
Ovidiu Ghita, John Mallon, Paul Whelan, *Dublin City University*
David Vernon, National University of Ireland Maynooth